Continental Shelf Research 145 (2017) 32–42

Contents lists available at ScienceDirect

Continental Shelf Research

journal homepage: www.elsevier.com/locate/csr

The bottom water exchange between the Singapore Strait and the West Johor Strait

Yunfang Sun[a,*], Elfatih Eltahir[b], Paola Malanotte-Rizzoli[c]

[a] Department of Earth, Atmospheric & Planetary Sciences, Massachusetts Institute of Technology, 77 Massachusetts Avenue, Building 54-1417, Cambridge, MA 02139, USA
[b] Department of Civil and Environmental Engineering, Massachusetts Institute of Technology, 15 Vassar Street, Room 48-207, Cambridge, MA 02139, USA
[c] Department of Earth, Atmospheric & Planetary Sciences, Massachusetts Institute of Technology, 77 Massachusetts Avenue, Building 54-1416, Cambridge, MA 02139, USA

ARTICLE INFO

Keywords:
Bottom circulation
Drifter trajectories
Singapore strait
West Johor Strait

ABSTRACT

As a part of the border between Singapore and Malaysia, the West Johor Strait (WJS) suffered newly from harmful algal blooms. There is no previous study showing the source of the nutrients in the WJS. This paper is investigating the possible water exchange between the water in the WJS and the bottom water in Singapore Strait.

This paper adopts a two-level nesting atmosphere-ocean coupled models to downscale the global atmosphere-ocean model into the Singapore coastal water, keeping the large-scale and long-term ocean and climate circulation signals and the advantages of the high-resolution. Based on the high-resolution ocean circulation fields, a Lagrangian particle tracking model is used to trace the Singapore Strait's bottom water movement and the water mixing in the WJS.

The results showed that the numerical models well resolved the Singapore coastal water regional circulation. There is a small but significant bottom water (1.25%) transport from the Singapore Strait to the WJS, which occurs from the southwest coastline of Singapore. The bottom water in the Singapore Strait prefers to enter the WJS during the spring tide and the flood period, and stay in Johor Strait for 6.4 days. The spring tide is the first-order factor for the water vertical mixing in the WJS, the wind is also very important for the vertical mixing especially in neap tide condition. An overall very important factor is the light perturbation. With the strongest vertical mixing of nutrients and bottom sediments due to the spring tide, the latter ones may inhibit the light penetration during the spring tide and reduce the algal bloom. The light penetration otherwise is greater during the neap tide, when the winds are the most important factor and hence favor the algal bloom. With the strongest wind in February and the longest permanence time in June and the sufficient nutrient supply in February and June, the most serious algal blooms may happen in February and June in the WJS.

1. Introduction

The Singapore island is located at the most important waterway between the Pacific and Indian Oceans, and in the equatorial tropics of the South China Sea. Due to its geographic position, the port of Singapore is a popular global trans-ship hub and the second busiest port in the world with ~3700 ships passing through it every day (MPA, 2017). Since the Republic of Singapore was found in 1965, the coastal environment has been changed dramatically over the last 50 years (Sien et al., 1988). Although Singapore's population density is already the highest in the world, the population of Singapore still continue to rise. As the existing land is limited, in order to meet the demands of growing population and booming of urbanization, multiple land reclamation and deep tunnel sewerage projects have been implemented, there are continuing changing the coastlines and the seabed, and reducing the biodiversity in the coastal waters. The land area of Singapore was 581.5 km^2 in the 60 s, 621.0 km^2 in the 80 s, and is now 719.1 km^2. Since its independence, the land reclamation has increased the total area by 23.7%, and extensive land reclamation projects are still ongoing. In order to save water and land resources, deep tunnel sewerage system projects (DTSS) (PUB, 2016) have been implemented to integrate the collection, treatment, reclamation and disposal of used water from industries, homes and businesses underground This process started at 2001. In June 2009, Phase 1 of DTSS

* Corresponding author.
E-mail addresses: yfsun@mit.edu (Y. Sun), eltahir@mit.edu (E. Eltahir), rizzoli@mit.edu (P. Malanotte-Rizzoli).

http://dx.doi.org/10.1016/j.csr.2017.07.004
Received 12 April 2017; Received in revised form 10 July 2017; Accepted 12 July 2017
Available online 17 July 2017

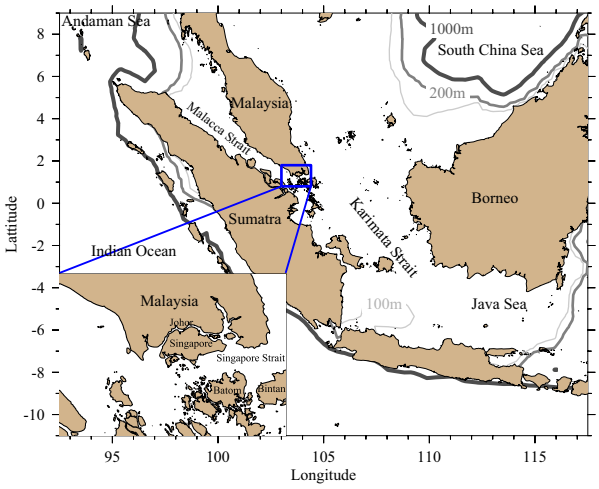

Fig. 1. The study regions including the South China Sea, the Malacca Strait, the Singapore Strait, and the Johor Strait.

was finished and started to discharge the waste water into the Singapore Strait through two 5 km long deep sea outfall pipes from the Changi Water Reclamation Plant.

Besides Singapore's local coastal environment changes, there is heavy traffic in the Singapore Strait, a channel between the Malacca Strait and South China Sea, connecting the Indian and Pacific Oceans (Fig. 1). It provides a deep-water passage to the Singapore Port. Although there is an International Convention for the Control and Management of Ships' Ballast Water and Sediments (BWM) (Andersen et al., 2011), which aims to prevent the spread of harmful aquatic organisms, the BWM regulation will be fully implemented only on 2020. Now ballast water with treatments can be discharged into the strait at a distance of 3 nautical miles or more from the nearest land (SSO, 2008), which may cause high risks for potential water pollution in the Singapore Strait (Xu and Chua, 2016).

The West Johor Strait (WJS) is a semi-enclosed narrow strait and acts as part of the border between the Malaysia Peninsula and Singapore. Harmful Algal Blooms (HABs) were observed in WJS, in June 2013, February 2014 and 2015. There are tons of waste water and ballast water discharges inside and into the Singapore Strait. The sewage discharge contains the nutrients necessary for dinoflagellate growing, and the ballast water contains both aquatic organisms and inorganic nutrients to support phytoplankton growing. If water containing the nutrients in the Singapore Strait could enter the WJS, and mix inside it, it will increase the risk of HABs in WJS, especially when there are leaks or accidents in the Singapore Strait. The tidal forcing is the main factor for the vertical mixing (Behera et al., 2013).

As the sea level in the South China Sea is about 0.15 m higher than in the Andaman Sea (Twigt, 2007; Hasan et al., 2016), there is a persistent and dominant westward flow in the Singapore Strait. Compared with other factors, tidal forcing plays the most important role in the coastal circulation (Chen et al., 2014b; Hasan et al., 2016). However, the circulation in Singapore coastal waters is not only affected by local factors, but also controlled by the remote global circulation variability, such as the monsoon wind system and El Niño Southern Oscillation (ENSO) (Sien et al., 1988; Behera et al., 2013; Kurniawan et al., 2015; Tay et al., 2016). The monsoon and ENSO's signals vary in strength and timing (Giese and Ray, 2011), providing uncertainty to predict the local circulation. The constructions' effects on the coastal waters have been well studied and evaluated by Singapore-Delft Water Alliance (SDWA) and Danish Hydraulic Institute (DHI) (DHI, 2007). However, the coastlines of Singapore are always changing, and there is no study of the water exchange between the Singapore Strait and WJS.

The Coupled Model Intercomparison Project Phase 5 (CMIP5) and the nesting of a high resolution 3-dimentional atmosphere-ocean coupled model provide the possibility to study the regional water circulation in a global domain with all the large-scale signals. By 2-level nesting, we could downscale the global model simulations to a 50 m resolution coastal ocean model. The Lagrangian particle trajectories can simulate the water and phytoplankton's sources and travel times (Tremblay et al., 1994; Garcia-Martinez and Flores-Tovar, 2000; Tian et al., 2009; Gilbert et al., 2010; Qiu et al., 2011; Dietrich et al., 2012). Four basic questions are asked: 1) What is the likelihood that the water at the bottom of the Singapore Strait can enter the WJS? 2) How long will this transport take? How long will this water stay inside the WJS 3) What are the effects of the wind on the mixing compared with the tide in the WJS? Can the wind be equally important as the tide in vertically mixing the water mass? 4) How important is the light penetration factor combined with the vertical mixing for the algal bloom? These questions have not been quantitatively addressed before.

The paper is organized as follows. In Section 2, the numerical models and the designs of numerical experiments are described. In Section 3, model results are presented. In Section 4, the major findings are discussed. In Section 5, a final summary is presented.

2. Data and methodology

2.1. Study region

The study regions are concentrated on the coastal waters around the Singapore Island, including the Singapore Strait and WJS, and are shown in the small panel of Fig. 1. The Singapore Strait is a 105-kilometer long, 16-kilometer wide, bounded by the Southern coastline of the Singapore Island, the Johor Shoal and the Southeastern coast of the Malay Peninsula on the north, Batam and Bintan Islands in the South. It connects the Strait of Malacca in the west and the South China Sea in the east. The Johor Strait is an international strait, separating the Malay Peninsula in the north, and Singapore in the south. There are two bridges crossing the strait: the Johor-Singapore Causeway and Malaysia-Singapore Second Link bridge. The Johor-Singapore Causeway cuts the water flow and separates the Johor Strait into the WJS and the East Johor Strait (EJS).

In previous studies, the Singapore Strait and WJS are controlled by the monsoon induced currents superimposed on the tidal ones (Sien et al., 1988, Hasan et al., 2016). During the northeast monsoon, a branch of the southward current from the South China Sea moves along the east coast of the Malaysia Peninsula and turns around at its southern tip to move into the Singapore Strait before entering the Strait of Malacca. During the southwest monsoon, a northward current from the Java Sea passes into the Singapore Strait and then enters into the Malacca Strait. Thus, there is always a westward flow in the Singapore Strait, but the water comes from the South China Sea during northeast monsoon and from the Java Sea during the southwest monsoon.

2.2. Numerical models

2.2.1. The South China Sea Coupled FVCOM/MRCM Model (SCSCM)

In order to include the global atmosphere and ocean circulation signals, a South China Sea coupled model is developed nested in the global model of the University Corporation for Atmospheric Research Community Climate System Model4 (UCAR-CCSM4). The UCAR-CCSM4 is a coupled model with a resolution of 1.25° × 0.94° used to simulate the earth's climate system, and includes atmosphere, ocean, land surface and sea-ice models.

The atmosphere-ocean coupled model over the Maritime Continent was developed by Wei et al. (2013), coupling the Finite Volume Coastal Ocean Model (FVCOM2.7) (Chen et al., 2003, 2006) as the oceanic component and the Regional Climate Model3 (RegCM3) (Giorgi and Mearns, 1999; Pal et al., 2007) as the atmospheric component via the

Ocean Atmosphere Sea Ice Soil coupler, version 3 (OASIS3) (Valcke, 2013). Xue et al. (2014) tested the local feedback mechanisms in the shallow water region by using this model. Based on the same structure and construction, we couple the MIT Regional Climate Model (MRCM) as the atmospheric component and the FVCOM3.1 as the oceanic component over the South China Sea region, obtaining the South China Sea Coupled MRCM/FVCOM Model (SCSCM).

MRCM was developed from RegCM3, improving the schemes of RegCM3 by coupling with the Integrated Biosphere Simulator (IBIS) land surface scheme (Winter et al., 2009), a new surface albedo prescription (Marcella and Eltahir, 2014c), a new irrigation scheme (Im et al., 2014), a new convective cloud scheme (Gianotti and Eltahir, 2014a), a new convective rainfall auto conversion scheme (Gianotti and Eltahir, 2014b), and modifying the boundary layer height and the boundary layer cloud scheme (Gianotti, 2013).

FVCOM was originally developed by Chen et al. (2003) and improved by the joint UMassD and WHOI FVCOM development team (Chen et al., 2013). For the details of FVCOM see the FVCOM User Manual (Chen et al., 2013). The finite volume unstructured grid system of FVCOM is ideal for geometrical fitting and topological flexibility, and made it particularly suitable applications in estuarine and coastal areas featuring complex coastlines and steep topographies (Chen et al., 2011, 2014a; Sun et al., 2013, 2016).

In the SCSCM, MRCM is configured to cover a domain between 93°E and 10°S and 120°E and 9°N with 12 km resolution and a 245×166 grid (left panel of Fig. 2). The surface pressure and wind components, air temperature, vertical velocity, relative humidity, and geopotential height at all vertical sigma levels from the historical simulation of UCAR-CCSM4 are used lateral boundary conditions for MRCM. The MRCM's time step is 120 s, and the radiation scheme and land surface scheme are integrated every 30 min and every 360 s, respectively.

In FVCOM of the SCSCM, the ocean domain covers the South China Sea and the Malacca Strait (blue grid in the left panel of Fig. 2), with a horizontal resolution varying from 3 km in the coastal regions to 27 km in the open ocean. A hybrid terrain-following coordinate is used in the vertical with a total of 30 layers. In water depths > 90 m, 5 uniform layers with a thickness of 3 m each are specified in the upper 15 m, while in regions with water depth ≤ 90 m, a sigma-coordinate is used with uniform layer thickness. The two vertical layer thickness schemes match at the water depth of 90 m. This hybrid coordinate is designed to ensure the accurate simulation of the surface mixed layer and bottom boundary layer over areas with strong bottom slopes. The bathymetry (Left panel of Fig. 3) is from General Bathymetric Chart of the Oceans (GEBCO) with a resolution of 30 arc second resolution (Becker et al., 2009). The open boundary conditions of Sea Surface Height (SSH), and Temperature/Salinity (T/S) are also from UCAR-CCSM4. Besides the long-term signals, tidal forcing is added into CCSM4, which are from TPXO7.2 (M_2, S_2, K_1, and O_1) (Egbert and Erofeeva, 2002). Its time step is 300 s.

The SCSCM's simulation period is from 1975 to 2005, which is following UCAR-CCSM4's historical simulation. The initial conditions for both MRCM and FVCOM are directly interpolated from UCAR-CCSM4 in December 1974. The coupling scheme is kept as in Wei et al. (2013). For the coupled MRCM, SST is initialized with OISST dataset and then updated every 6-h through OASIS3 from SST simulated by FVCOM; at the same time, FVCOM receives the heat fluxes and surface wind speed every 6-h from MRCM.

2.2.2. High-resolution Singapore coastal ocean model (Sin-FVCOM)

The SCSCM brings the large-scale signals into the Singapore coastal region. As there is only one layer of cells inside the WJS, this resolution cannot resolve the WJS. Then the high-resolution coastal ocean model has been developed, which is configured for the domain shown in the right panel of Fig. 2, with a horizontal resolution varying from 40 m near the Johor-Singapore Causeway to 3 km in the open boundaries at the Singapore and Malacca Straits. The computational domain of the Sin-FVCOM completely covers the whole Singapore island and the adjacent waters, well resolves the Johor-Singapore Causeway and resolves ~200 islands. It is also surrounded by an open boundary running across the Malacca Strait on the west, South China Sea in the east (right panel of Fig. 2). The bathymetry is based on the 2016 Admiralty charts (right panel of Fig. 3). A hybrid terrain-following coordinate is used in the vertical with a total of 15 layers. In water depths > 30 m, 5 uniform layers with a thickness of 2 m are specified in the upper 10 m, while in regions with water depth ≤ 30 m, a sigma-coordinate is used with uniform layer thickness. The two vertical layer thickness schemes match at the water depth of 30 m. We are using the 2016 coastal line and bathymetry, with the SCSCM providing the results for 1975–2005, to study the mechanisms and possible water exchange between the Singapore Strait and WJS. Therefore, we want to find an extreme monsoon year in the period of 1975–2005 to use as the forcing to drive the coastal circulation. As the strongest monsoon signal occurred in 1983 (Kajikawa and Wang, 2012; Watanabe and Yamazaki, 2014). Our simulation period for the Sin-FVCOM is January 1982 to March 1984. The year of 1982 is used for model spin-up. The initial T/S, SSH, velocity conditions in January 1st, 1982 are interpolated from the SCSCM results. The open boundary condition is one-way nested from the SCSCM's ocean component (SSH, T/S), the surface forcing is from the SCSCM's coupled atmospheric component (Wind speed, heat flux). The tidal constituents M_2, S_2, N_2, K_2, K_1, O_1, P_1, Q_1 from TPXO7.2 are used. The DTSS discharges and ballast water discharges from ships are not included in this coastal model, as their total influences for the physical circulation are less than 0.05% in the

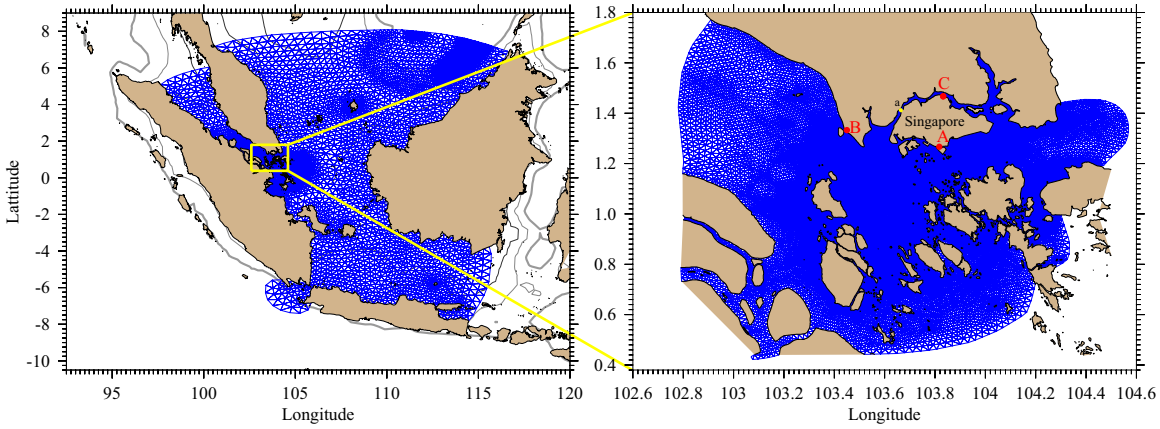

Fig. 2. The model domains: left panel: the whole box domain is the SCSCM's MRCM domain, the blue grid is SCSCM's FVCOM grid; right panel: the blue grid is the Sin-FVCOM grid, site A, B, C are 3 tidal gauge stations, site a is a site inside the West Johor Strait.

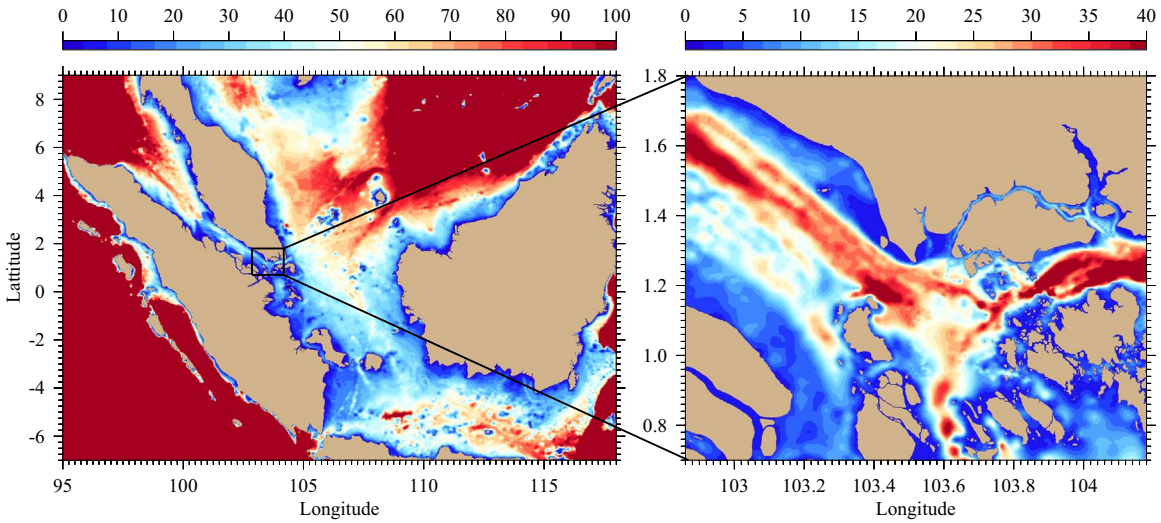

Fig. 3. The bathymetry of the study regions: left panel shows the bathymetry of the SCSCM; right panel shows the bathymetry of the Sin-FVCOM.

Singapore Strait. There are 2 major rivers in the Sin-FVCOM domain, which are the Johor River (Hasan et al., 2012; van Maren and Gerritsen, 2012) and Sungai Pulai (Behera et al., 2013). The yearly average discharges of the two major rivers are approximately 80 m^3/s and 45 m^3/s respectively, and the two river discharges are estimated by using the accumulated rainfall data in the surrounding catchment (Hasan et al., 2012), there is no monthly or annual discharge data available. The other hydrodynamic modeling in this region is using the two constant values with no seasonal or annual variation. The purpose of the coastal ocean model is to investigate the monthly variations, and the river discharges account for less than 0.2% variation in the circulation. Therefore, the rivers are not included in the Sin-FVCOM.

The tidal constituents of the Sin-FVCOM are validated by using the hourly SSH data of 3 tidal gauge locations (Table 1) from the University of Hawaii Sea Level Center (UHSLC, http://uhslc.soest.hawaii.edu/), and the data are analyzed by t_tide (Pawlowicz et al., 2002).

By comparing the observation and model results (Table 2), the mean M_2 amplitude difference is 0.3 cm, the phase difference is less than 6°, the S_2 mean amplitude difference is 1.3 cm, the phase difference is ~15°. All the mean phase difference for the 8 tidal constitutes used in the model is less than 30°. And all the mean amplitude differences are less than 7 cm. The M_2 tidal chart is shown in Fig. 4, the M_2 amplitude is higher in the west, lower in the east in the Singapore Strait, however in the WJS, the amplitude of M_2 is increasing from the west entrance of the WJS to the causeway, and the phase difference in the WJS is ~10°.

2.2.3. Lagrangian tracking model

As the hourly high-resolution flow fields are provided by the Sin-FVCOM, in order to trace the water movement, a Langrangian tracking model is used. The particle trajectories are simulated by solving the 3-D kinematic equations given as

$$\frac{d\vec{X}}{dt} = \vec{v}(\vec{X}(t),t) \tag{1}$$

Table 1
Tidal gauge names and locations.

ID	Station name	Longitude	Latitude	Time
A	Victoria Dock	103.817	1.267	1972–1981
B	Kukup	103.45	1.333	1985–2013
C	Johor Bahru	103.47	1.47	1983–2013

where $\vec{X}$ is the particle's position vector at a time t, $\vec{v}(\vec{X},t)$ is the 3-D velocity vector interpolated from the model, and t is the time. The kinematic equations for $\vec{v}$ is solved using the explicit Runge-Kutta (ERK) multi-step method which is derived from solving the discrete integral:

$$\vec{X}(t) = \vec{X}(t_n) + \int_{t_n}^{t} \vec{v}(\vec{X}(t),\tau)d\tau \tag{2}$$

This is an approximate discrete integration method with a truncation error of order $(\Delta t)^5$, where Δt is the integration time step. A detailed description of the particle tracking algorithm used in this method is given in the FVCOM User Manual (Chen et al., 2013).

The fourth-order Runge-Kutta method requires that the time step Δt is chosen to satisfy the criterion $\Delta tK < 0.05$, where K is an upper bound of the spatial gradient of velocity (Chen and Beardsley, 1998). The Singapore coastal region is dominated by the M_2 tide, so that K can be approximately by the M_2 tidal frequency ω. When 60 s (1 min) for Δt in the particle tracking experiments is chosen, then ΔtK yields $\Delta t\omega \approx 0.01$. Oliveira et al. (2002) also derived a criterion which the time step depended on the value of the Stokes number S_t. S_t is defined as $S_t = \tau^p/\tau$, where τ^p is the particle response time and τ is the fluid velocity response time. When S_t ~0.1 or less, the particle follows the fluid flow. Therefore, the time step Δt should be set up ~ 0.1τ~360 seconds for the hourly flow field. Considering the accuracy, 60 s is chosen to ensure tracking accuracy with no sacrifice in computational efficiency.

2.3. Design of numerical experiments

Based on the Sin-FVCOM's 1983 hourly ocean flow field, one must be aware of the limitation of the model in resolving spatial scales. 234 locations (Fig. 5) with 2 km intervals between each other are selected in the Singapore Strait to release particles. In the horizontal domain, the model resolution varies from ~50 m over the WJS and EJS and 200 m at the west entrance of the WJS to 1–3 km in the interior of the Malacca Strait and South China Sea. In the areas where drifters are deployed, the grid horizontal resolution ranges from 300 to 500 m. Since most of the drifters eventually move into the Malacca Strait, we need to consider the spatial scale resolved by the grid, which is about 500 m in this region. In the vertical, the model is configured with 15 layers. Considering the maximum depth of ~150 m in the Singapore Port, and the mean depth is ~15 m, the average vertical resolution is about 1.0 m. This

Table 2
Statistics of the comparison between model-computed and observed tidal elevations at the 3 tidal gauges (Magnitude in meter, phase in degree).

Tide	Station A				Station B				Station C			
	Observation		Model		Observation		Model		Observation		Model	
	Magnitude	Phase	Magnitude	Phase	Magnitude	Phase	Magnitude	Phase	Magnitude	Phase	Magnitude	Phase
M_2	0.798	79.7	0.730	95.1	0.936	92.4	0.980	89.6	0.792	94	0.801	100.2
S_2	0.327	125.3	0.308	147.6	0.429	137.2	0.510	154.8	0.324	138.6	0.300	143.3
K_1	0.289	350.3	0.240	325.8	0.259	42.4	0.232	61.8	0.308	352.3	0.250	353.4
O_1	0.289	306	0.190	335.82	0.254	7.6	0.194	18.6	0.301	306.7	0.253	349.3
N_2	0.159	61.2	0.245	81.9	0.171	81.4	0.271	82.0	0.156	73.5	0.180	97.5
K_2	0.099	123.6	0.138	157.4	0.129	132.6	0.178	152.4	0.096	137.8	0.114	162
P_1	0.091	343.5	0.034	355.7	0.079	33.1	0.032	36.0	0.097	343.4	0.045	348.3
Q_1	0.056	274.4	0.025	255.2	0.041	329.7	0.016	300.9	0.062	273.1	0.032	242.5

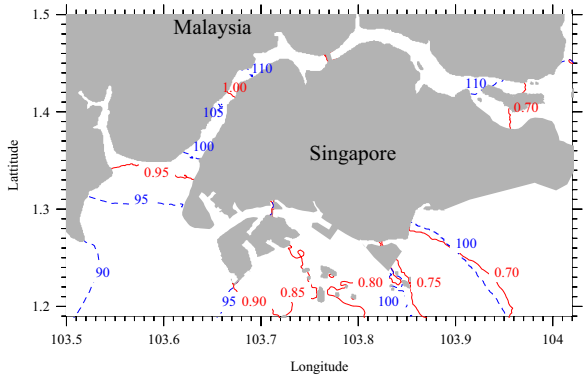

Fig. 4. M_2 tidal chart in the Singapore coastal region. The red solid lines are the amplitude of M_2 in meter; the blue dash lines are the phase of M_2 in degree.

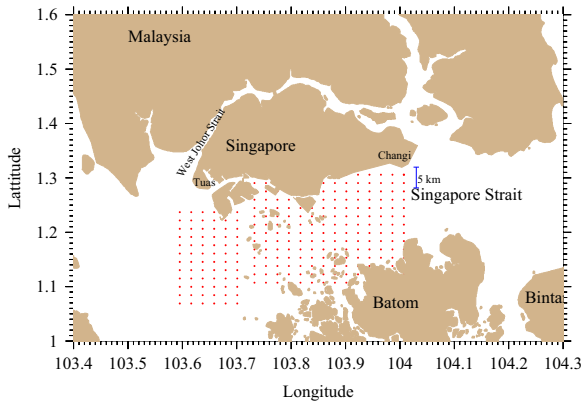

Fig. 5. The red dots are the deployed particles' initial locations; the blue segment shows the scale of 5 km. (For interpretation of the references to color in this figure legend, the reader is referred to the web version of this article.)

resolution is sufficient to resolve the vertical structure of the flow, particularly in this shallow water region. The focuses are on the bottom waters in the Singapore Strait, as the heavier pollutions in seawater from ballast discharges sinks to the bottom, and bottom efficient discharges will accumulate the nutrients in the bottom. The particles are released 0.5 m above the bottom at each location, ensuring that the initial location is in the bottom layer; after releasing, the particles can move horizontally and vertically following the adjacent flow.

One particle is released from the selected 234 locations every hour in 1983, and each particle is traced for 3 months. Therefore, we have 234*8760 particle trajectories to analyze the water movements.

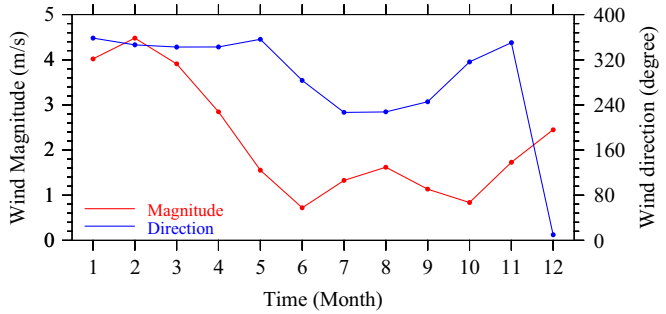

Fig. 6. The 30-year average wind magnitude and direction around the Singapore island calculated from the SCSCM.

3. Results

3.1. Circulation pattern

From the SCSCM's atmospheric part, the 30-year monthly wind variation around the Singapore island is shown in Fig. 6. In February, the northeast wind is strongest; In August, the southwest wind is strongest; June and November are the transition periods. The wind simulated from SCSCM is compared with ERA-Interim (Berrisford et al., 2011), which is ECMWF (European Center for Medium-range Weather Forecasts) Re-Analysis Interim (Data is available from 1979 to present with a horizontal resolution of 0.75° × 0.75°). The SCSCM's model results and the original CCSM4's outputs are monthly averaged to the ERA-Interim grids for the period of 1979–2005 in the SCSCM's MRCM domain (Fig. 2a). The wind magnitude from both the CCSM4 and SCSCM are larger than the wind estimated from ERA-Interim. CCSM4 is 30.8% larger than ERA-Interim. Compared to CCSM4, SCSCM is better than CCSM4, being only 24.2% larger than ERA-Interim. The standard deviation of the differences between CCSM4 and ERA-Interim and between SCSCM and ERA-Interim are 1.07 m/s and 1.02 m/s respectively. The direction difference is 8° between ERA-Interim and CCSM4. The direction difference is 15° between ERA-Interim and SCSCM. It means that the SCSCM has better wind magnitude simulation results than CCSM4, but due to the coarse resolution of ERA-Interim and CCSM4, the wind direction is not as well as CCSM4. From the SCSCM's oceanic part, the monthly averaged surface current shows that in the northeast monsoon, one part of the southward South China Sea Through Flow (SCSTF) (Gordon, 2005, 2012) turns west to enter the Singapore Strait, and eventually goes northwards into the Malacca Strait; in the southwest monsoon at the surface, the SCSTF goes northward, the westwards currents from the Java Sea enter the Singapore Strait, and then move again into the Malacca Strait. The monthly mean bottom circulation also shows the westward currents in the Singapore Strait, but the current speed is much lower than at the surface. In the southwest Monsoon, however,

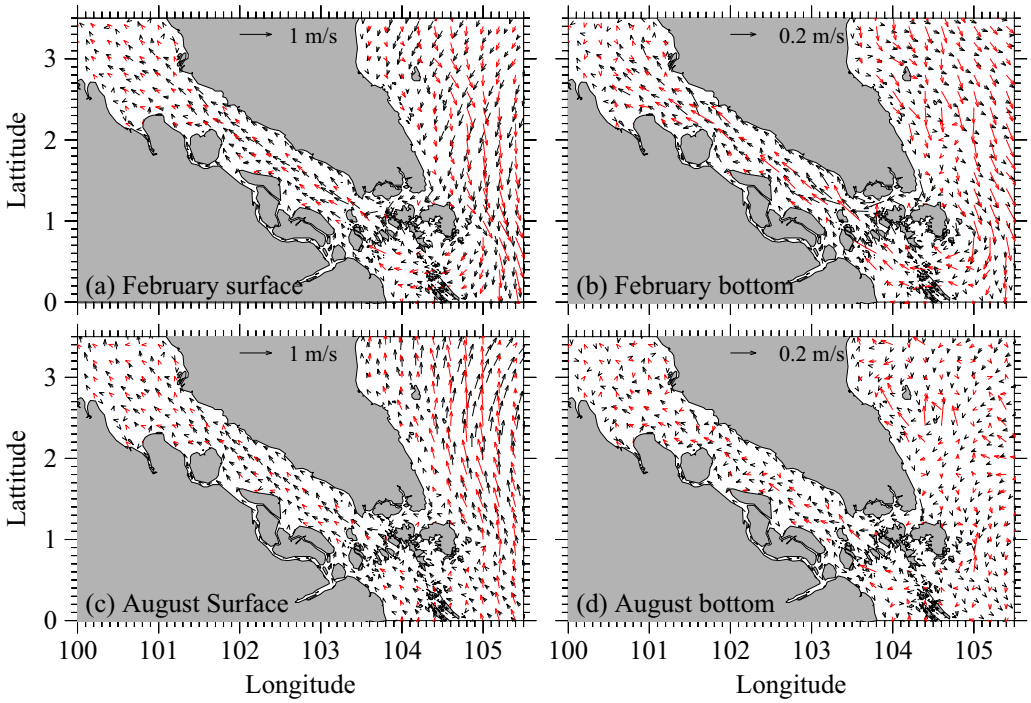

Fig. 7. The 1982–1984 monthly mean surface currents in February (a), August (c), bottom currents in February (b), August (d), black arrows are calculated from the SCSCM; red arrows are calculated from the OFES. (For interpretation of the references to color in this figure legend, the reader is referred to the web version of this article.)

Table 3
The Absolute velocity differences between SODA, SCSCM and OFES (1976–2005).

Direction	SODA–SCSCM		SODA - OFES		OEFS - SCSCM	
	Mean[a]	Std[b]	Mean	Std	Mean	Std
Surface (East-west)	0.14	0.03	0.07	0.02	0.11	0.02
Surface (North-south)	0.13	0.02	0.07	0.02	0.13	0.03
Bottom (East-west)	0.03	0.01	0.02	0.01	0.05	0.01
Bottom (North-south)	0.03	0.01	0.04	0.01	0.04	0.01

[a] Mean is the absolute mean velocity difference, unit is m/s.
[b] Std is the standard deviation of the absolute mean difference, unit is m/s.

the bottom water circulation in the Java Sea is different from the surface currents. The surface and bottom velocity fields are compared with Simple Ocean Data Assimilation (SODA), which is a monthly averaged global ocean dataset from 1871 to 2010 with a resolution of 0.5° × 0.5° (Giese and Ray, 2011; NCAR, 2016). OFES is a monthly averaged global ocean dataset from 1950 to 2014 with a resolution of 0.1°×0.1° (Masumoto et al. 2004; Sasaki et al. 2008). This circulation patterns of the SCSCM and OFES are shown in Fig. 7, both consistently with previous studies, the main patterns of the two models are very similar. The absolute difference for the monthly surface and bottom current velocities of the period of 1976–2005 are shown in Table 3. The difference between OEFS and SODA and the difference between

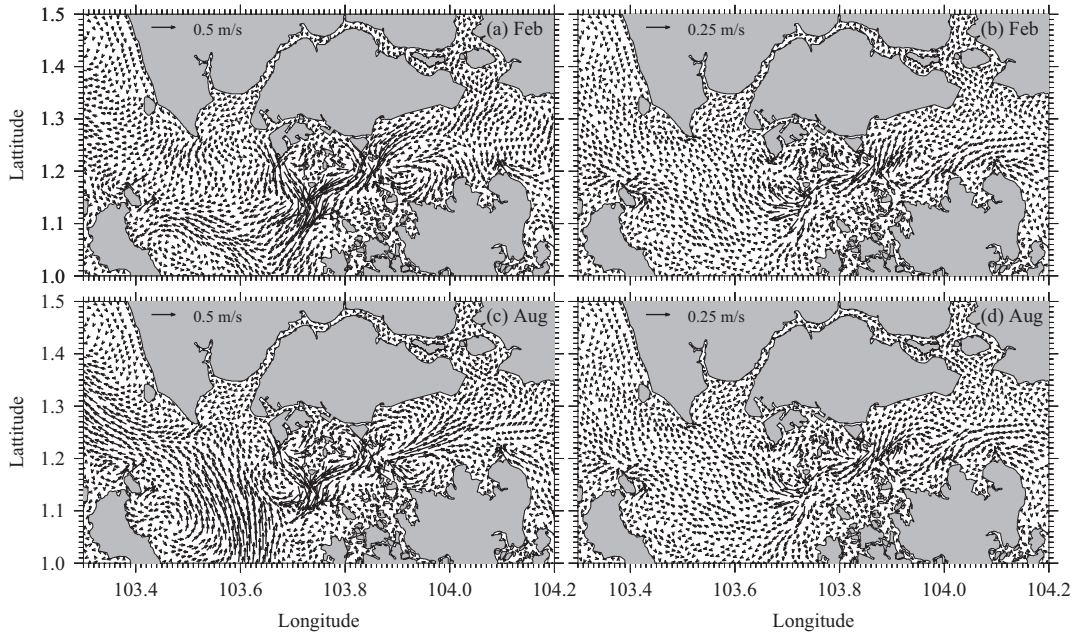

Fig. 8. The monthly mean surface currents in February 1983 (a), August 1983(c), bottom currents in February 1983 (b), August 1983 (d), calculated from the Sin-FVCOM.

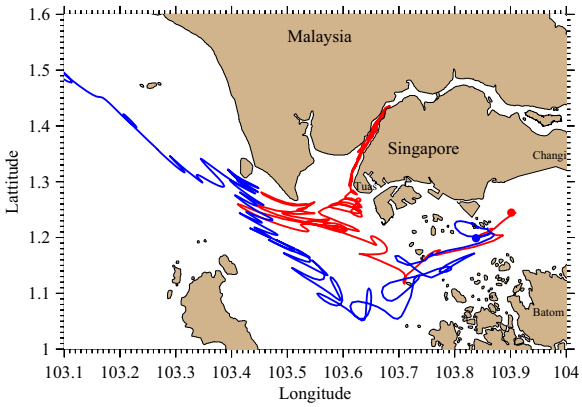

Fig. 9. The red line and blue line are the examples of the particle's typical trajectories from the Lagrangian model simulations. (For interpretation of the references to color in this figure legend, the reader is referred to the web version of this article.)

SCSCM and SODA are in the same order, 10 cm/s in surface velocity, and 3 cm/s in bottom velocity.

Fig. 8 presents the monthly average circulations from the high-resolution Sin-FVCOM results, also showing the consistent westward currents in the Singapore Strait. Due to the high resolution and accurate coastline and bathymetry, many eddies are resolved, which are not apparent in the SCSCM. And the northward currents into the Malacca Strait is also evident. At the surface, the monthly mean currents are always flowing from the WJS to the Singapore Strait, never in the opposite way. However, in the bottom, some currents at the South of the Jurong island can continuously enter the WJS.

3.2. Drifter simulation results

Two typical kinds of particle trajectory are illustrated in Fig. 9: the majority (more than 95%) of particles behave as shown in the blue trajectory, the particle meanders southwestwards in the Singapore Strait, and then turns northwestwards to the Malacca Strait. The back and forth fluctuations are due to tidal forcing. A small portion (less than 5%) of particles follow the red trajectory, the particle turns eastward near the tip of the Malaysia peninsula, and then stays in the WJS. The particles remain in the bottom inside the Singapore Strait, but they can have strong upwelling and downwelling in the WJS.

3.3. Spatial and temporal probabilities

To confirm that some particles enter the WJS and stay inside, the

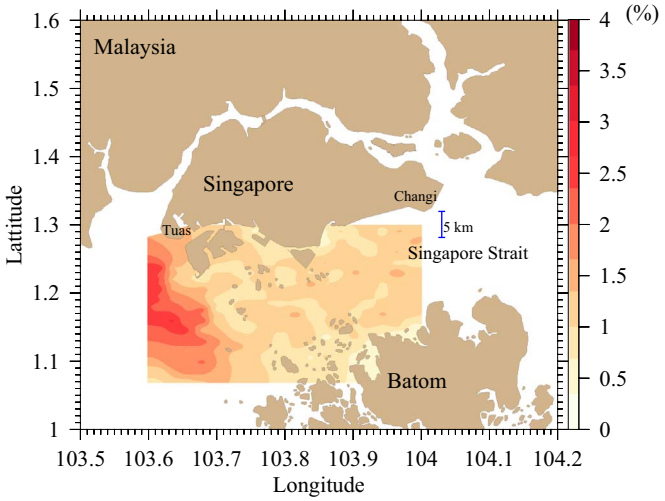

Fig. 10. The percentage of particles which enter the WJS over all particles released.

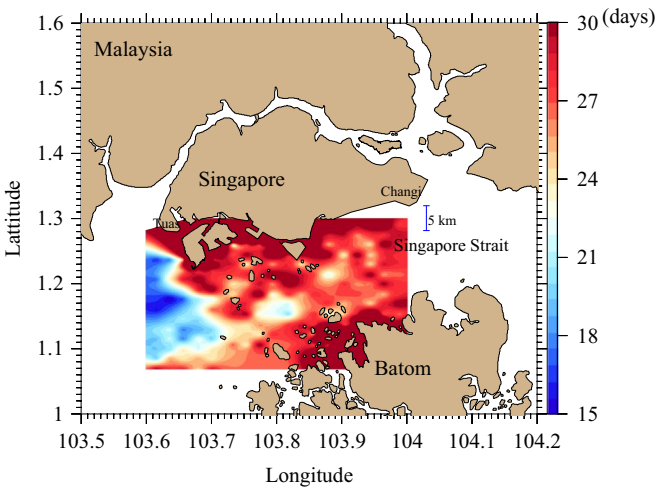

Fig. 11. Time for particles taken to enter the WJS from the locations released.

percentage of the particles among all those released is calculated and shown in Fig. 10. The percentage is not uniformly distributed, and not even related to the water depth, the highest percentage (about 4%) occurs near the south of Tuas and the Jurong island at the location; where the red particle changes its direction in Fig. 9. There are also some very favorable positions located South of the Changi Water Reclamation Plant. The average probability in the whole field is ~1.25%. Although this value is small, as there are totally 2,049,840 particles deployed in the experiment, 1.25% of these is ~25600 particles entering the WJS, so they can't be ignored.

The particles' travel time from the release position to the entrance of the WJS is estimated from the particle's trajectories, and shown in Fig. 11. South of Tuas, where the probabilities of entering the WJS is highest, it takes ~15 days; for the low probability region, it may take as long as one month for the particles to enter. As Changi and Tuas are the two effluent underwater discharges in the DTSS projects, Fig. 10 and Fig. 11 show that there is a high probability for the bottom waters at the two locations with sewage discharge to enter the WJS within one month.

The temporal distribution for the particles entering the WJS in different months is investigated by evaluating the normalized probability, which is shown in Fig. 12. The result shows that in February, March, April, May and June, the probabilities are above the average, with the peak in May, while in other months, they are below the average. Therefore, there are more chances of algal blooms in February, March, April, May and June. Fig. 13 shows the average permanence time for the particles wading the middle of the WJS measured from the initial entering time. The total averaged permanence time is 6.4 days. During the year, June has the longest permanence time with an average value of 8.8 days. Combining the permanence time (Fig. 13) and the entering probability (Fig. 12), June is the most favorable month for the bottom water rich of sewage nutrients to produce algal blooms in the WJS.

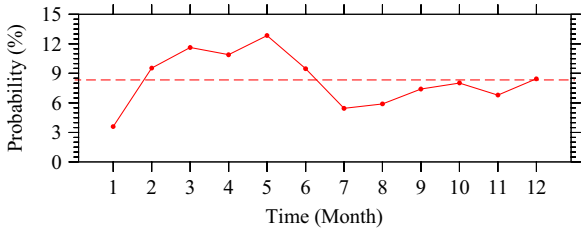

Fig. 12. The red solid line shows the temporal normalized probabilities for particles which can enter the WJS; the red dash line shows the average probabilities, which is 1/12. (For interpretation of the references to color in this figure legend, the reader is referred to the web version of this article.)

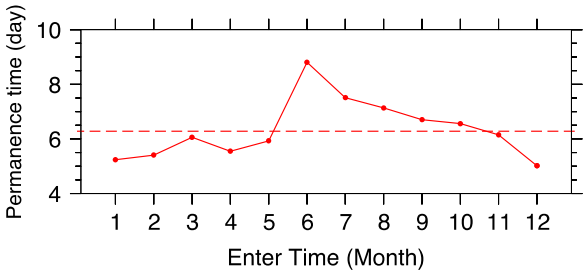

Fig. 13. The permanence time for particles staying inside the WJS.

4. Discussion

4.1. Physical conditions favoring paticle entering the WJS

The tide and the wind are the two most important factors for the circulation in the study region, hence their conditions for favoring the particles to enter the WJS are investigated. The spring tide is characterized by a water level amplitude larger than 1.6 m at the west entrance of the WJS, and the neap tide by a water level amplitude less than 1.4 m at the same location. Fig. 14a shows that 45.4% of the particles enter the WJS during the spring tide, and 28.9% enter during the neap tide, with the spring tide favoring a much larger entrance of the particles. Fig. 14b shows that 83.6% of the particles enter at the flood period, and no particle enters during the ebb period. The usual spring and neap tide period is ~14 days. As the particles can stay in the WJS for about 6.4 days, if the particle enters the WJS during the spring tide, as it is most probably, after 6.4 days it will encounter the condition of the neap tide.

Regarding the wind condition, as shown in Fig. 6, the winds in most of the time are from the northeast direction around the Singapore Island. The wind distribution in 1983 shown in Fig. 15 is similar to the 30-year averaged wind. The blue dots in Fig. 15 show all the hourly wind, and the red dots show the winds when the particles enter the WJS. Comparing the ratio of winds favorable to the entering of particles and all the wind, all of the ratios are between 0.9 and 1.1, meaning that the particles enter the WJS with no significant preference for the wind conditions, except it has the lowest ratio of 0.7 when the wind is in the northwest direction (Table 4).

Fig. 16 shows the typical scenarios of the particle entering the WJS from the bottom water of the Singapore Strait in the flood period of the spring tide. The northeastward inflow from the Malacca Strait enters the WJS, the eastward velocity is strong both in the Malacca Strait and the WJS, pushing the water to enter the WJS; in the following ebb period, the strong currents from the Singapore Strait flow northwestward into the Malacca Strait, and join with the southward weaker outflow currents from the WJS. The pattern of the bottom current indicates that the particles enter the WJS in one tidal cycle.

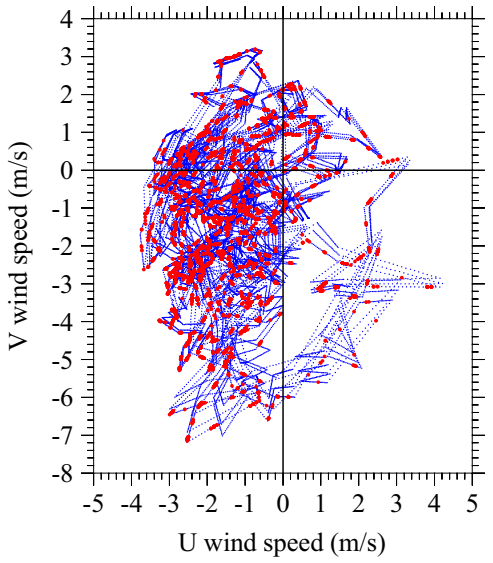

Fig. 15. The blue dots shows the hourly wind in the year of 1983; the red dots are the winds when particles enter the WJS. (For interpretation of the references to color in this figure legend, the reader is referred to the web version of this article.)

Table 4
The ratio of winds favorable to the entering of particles and all the wind of Fig. 15.

Wind direction	Wind direction percentage (red)	Wind direction percentage (blue)	Ratio between column 2 and column 3
Southwest	6.4%	6.1%	1.1
Southeast	19.4%	21.9%	0.9
Northeast	68.0%	63.6%	1.1
Northwest	6.2%	8.4%	0.7

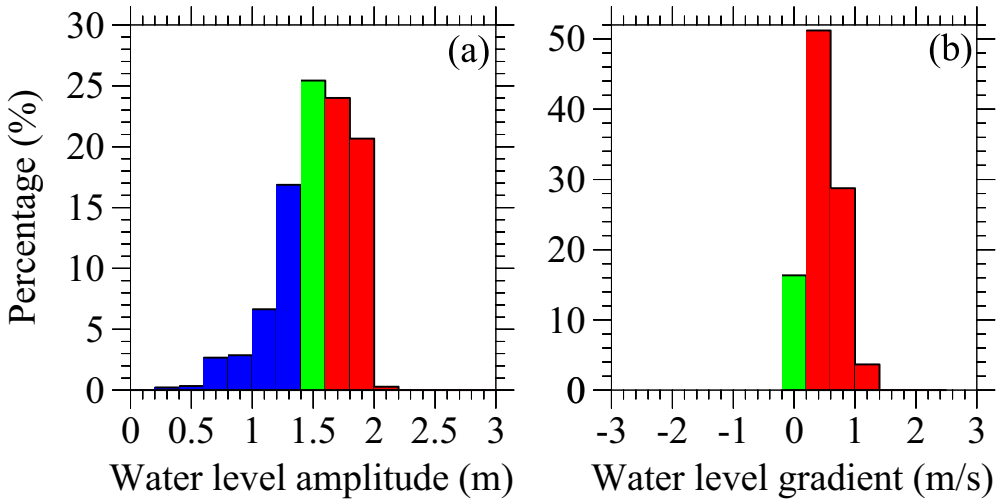

Fig. 14. The tidal conditions for the particles entering the WJS: in panel a, red represents spring tide, blue represents neap tide, green is between spring and neap tide; in panel b, red represents the flood period, blue represents the ebb period, green represents the period between flood and ebb, there is no blue bar from statistics. (For interpretation of the references to color in this figure legend, the reader is referred to the web version of this article.)

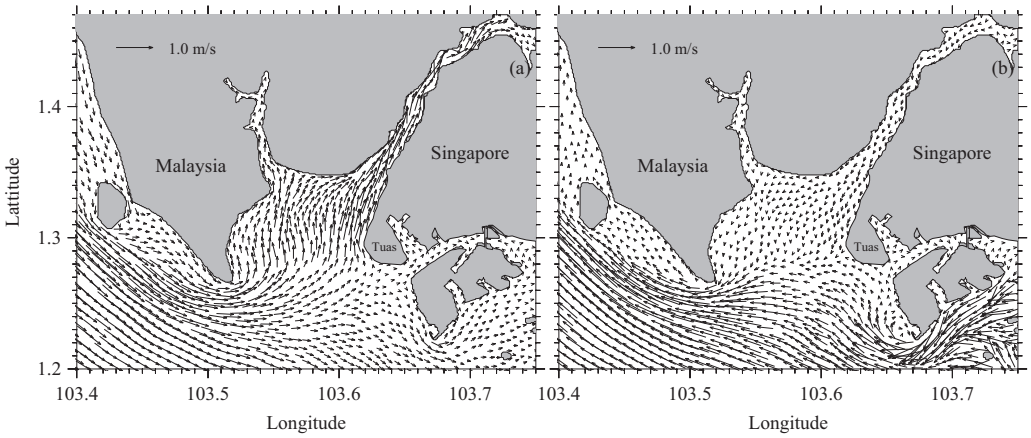

Fig. 16. The typical bottom currents conditions when the particles enter the WJS: panel a shows the flood period of spring tide; panel b shows the ebb period of the same spring tide.

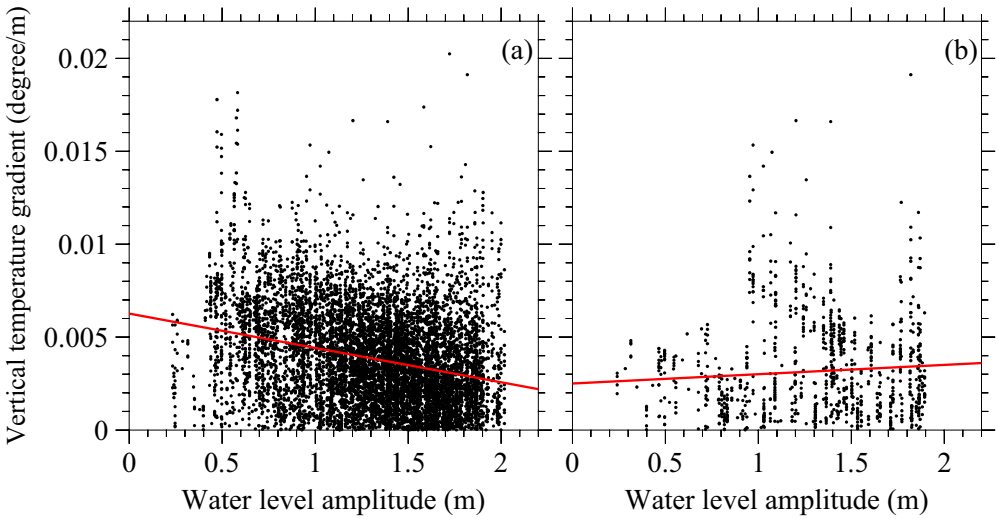

Fig. 17. In panel a, the black dots are scattered based on the water level amplitude (x axis) and vertical temperature gradient (y axis) at site a in the year of 1983, the red line is the least square fitting for the black dots; in panel b, the black dots is selected from panel a when the wind speed is larger than 5 m/s in 1983, the red line is also is the least square fitting for the black dots. (For interpretation of the references to color in this figure legend, the reader is referred to the web version of this article.)

4.2. Mixing in West Johor Strait

If the entering water always stays at the bottom in the WJS, it won't provide nutrients to the algae in the upper layer of the WJS, and there will be no algal blooms. As there are frequent algal blooms, there must be strong vertical mixing in the WJS. Then the tide and the wind effects on the mixing are investigated separately.

The internal vertical mixing in the WJS is strongest due to the tidal forcing, as observed by Behera et al. (2013). This phenomenon is confirmed by the numerical results in Fig. 17, In the left panel, the red line's slope is negative (−0.002), meaning that when the water level amplitude is largest (in spring tide), the vertical temperature gradient is smaller (intense vertical mixing), on the other side, when the water level amplitude is smaller (in neap tide), the vertical temperature gradient is larger (poor vertical mixing). This suggests that the spring tide produces strong mixing at site a in the WJS.

For the wind's contribution to mixing, considering the wind speed magnitude and including all the wind speeds in 1983, the mixing is again strong during the spring tide, and weak during the neap tide, as shown in Fig. 17a. However, if only the larger wind speeds are considering (> 5 m/s), the slope of the red line in Fig. 17b becomes slightly positive. This means that with the strong winds, the water mass can be vertically well mixed also in neap tide, and the winds are probably the major mixing agent in neap tide condition.

Light, temperature, nutrient supply are the three necessary conditions for algae growing (Russell, 1927; Banse, 1964; Postma and Rommets, 1970), A very important factor for algal blooms is a good light penetration and the strong vertical turbulence affects the light penetration. When the spring tide mixes the water vertically, the nutrients and sediments are upwelling to the surface from the bottom, the visibility becomes low, allowing less light to penetrate into the water. The algal may grow slowly during spring tide. During the neap tide period, the water is not well mixed by the tide. Without the high vertical turbulence, the light can penetrate downwards, the algal to grow fast, the nutrients source from the bottom are exhausted, then the algal stop growing, and wait for the next spring tide or a strong wind to mix the water again. The penetration of light explains the high chlorophyll-a concentration during the neap tide, and low chlorophyll-a concentration during the spring tide from the observation (Behera et al., 2013).

The extreme high chlorophyll-a concentration is the algal bloom. Combined with the nutrients supply, nutrients permanence and wind strength, it explains why the algal blooms occur in February and June, as there is strong supply in February, and the strongest wind and the tide produce strong vertical mixing in the WJS; In June, the nutrients supply from the Singapore Strait is also above the average, although the wind in June is the weakest in the year. Due to the longest particle permanence time, the spring tide causes the strong vertical mixing, providing the essential environment for the algal blooms.

5. Summary

The Singapore Strait is one of the busiest waterway in the world, thousands of ships go through the strait every day; tons of waste water are discharged via deep tunnels and ships into the Singapore Strait every day. Recently, HABs happened several times in the WJS. This paper shows a possibility that the bottom polluted water in the Singapore Strait can enter the WJS from the bottom water transport, and then cause the HABs.

By using the atmosphere-ocean coupled model SCSCM to downscale the global ocean, land surface and sea-ice coupled model (UCAR-CCSM4), the nested high-resolution Sin-FVCOM carries these large-scale and long-term signals to the Singapore coastal water, has well resolved the local coastal ocean circulation.

From the Lagrangian particle tracking model results, it shows that there is small but significant transport of the bottom water (1.25%) in the Singapore Strait, which can enter the WJS from the southwest coastline of Singapore.

The bottom water in the Singapore Strait prefers to enter the WJS during the spring tide and the flood period, and stay in it for ~6.4 days. The tide is the main contributor for the vertical water mixing in the WJS; at the same time, the wind (> 5 m/s) is also an important factor for the water vertical mixing especially in neap tide.

The light perturbation is an overall very important factor. With the strongest vertical mixing of nutrients and bottom sediments due to the spring tide, the latter ones may inhibit the light penetration during the spring tide and reduce the algal bloom. The light penetration otherwise is greater during the neap tide, when the winds are the most important factor and hence favor the algal bloom.

In February, there is high nutrients supply from the Singapore Strait, the strongest wind in the year helping the vertical mixing and the strong tidal mixing; in June, there is high nutrients supply from the Singapore Strait, and the longest permanence time and the strong tidal mixing. These factors in February and June encourage the most serious algal blooms in the WJS.

Acknowledgements

This work was supported by the Singapore National Research Foundation (NRF) through the Center for Environmental Sensing and Monitoring (CENSAM) under the Singapore-MIT Alliance for Research and Technology (SMART) program. We would like to thank Eun-Soon Im and Jun Wei for their valuable discussions.

References

Andersen, M., Chua, E., Casten, L.R., Drillet, G., 2011. Challenges and opportunities in developing a land based test facility for ballast water treatment systems in Singapore, International Maritime-Port Technology and Development Conference (MTEC2011), http://dx.doi.org/10.3850/978-981-08-7617-3_120.

Banse, K., 1964. On the vertical distribution of Zooplankton in the sea. Progress. Oceanogr. 2, 53–125. http://dx.doi.org/10.1016/0079-6611(64)90003-5.

Becker, J.J., Sandwell, D.T., Smith, W.H.F., Braud, J., Binder, B., Depner, J., Fabre, D., Factor, J., Ingalls, S., Kim, S.-H., Ladner, R., Marks, K., Nelson, S., Pharaoh, A., Trimmer, R., Von Rosenberg, J., Wallace, G., Weatherall, P., 2009. Global bathymetry and elevation data at 30 arc seconds resolution: srtm30_plus. Mar. Geod. 32 (4), 355–371.

Behera, M.R., Cui, C., Palani, S., Tkalich, P., 2013. Temporal variability and climatology of hydrodynamic, water property and water quality parameters in the West Johor Strait of Singapore. Mar. Pollut. Bull. 77 (1/2), 380–395. http://dx.doi.org/10.1016/j.marpolbul.2013.09.043.

Berrisford, P., Dee, D.P., Poli, P., Brugge, R., Fielding, K., Fuentes, M., Kållberg, P.W., Kobayashi, S., Uppala, S., Simmons, A., 2011. The ERA-Interim archive Version 2.0, ERA Report Series.

Chen, C., Beardsley, R.C., 1998. Tidal mixing and across-frontal particle exchange over a finite-amplitude asymmetric bank: a model study with application to Georges Bank. J. Mar. Res. 56, 1163–1201. http://dx.doi.org/10.1357/002224098765093607.

Chen, C., Liu, H., Beardsley, R.C., 2003. An unstructured grid, finite-volume, three-dimensional, primitive equations ocean model: application to coastal ocean and estuaries. J. Atmos. Ocean. Technol. 20 (1), 159–186. http://dx.doi.org/10.1175/1520-0426(2003)020.

Chen, C., Beardsley, R.C., Cowles, G., 2006. An unstructured grid, finite-volume coastal ocean model (FVCOM) system. Oceanography 19, 78–89. http://dx.doi.org/10.5670/oceanog.2006.92.

Chen, C., Huang, H., Beardsley, R.C., Xu, Q., Limeburner, R., Cowles, G.W., Sun, Y., Qi, J., Lin, H., 2011. Tidal dynamics in the Gulf of Maine and New England Shelf: an application of FVCOM. J. Geophys. Res. 116 (12). http://dx.doi.org/10.1029/2011JC007054.

Chen, C., Beardsley, R.C., Cowles, G., Qi, J., Lai, Z., Gao, G., Stuebe, D., Xu, Q., Xue, P., Ge, J., Ji, R., Hu, S., Tian, R., Huang, H., Wu, L., Lin, H., Sun, Y., Zhao, L., 2013. An unstructured grid, finite-volume community ocean model FVCOM user manual, SMAST/UMASSD Technical Report 13-0701, SMAST, UMassD, MA.

Chen, C., Lai, Z., Beardsley, R.C., Sasaki, J., Lin, J., Lin, H., Ji, R., Sun, Y., 2014a. The march 11, 2011 Tōhoku M9.0 earthquake-induced tsunami and coastal inundation along the japanese coast: a model assessment. Progress Oceanogr. 123, 84–104. http://dx.doi.org/10.1016/j.pocean.2014.01.002.

Chen, H., Malanotte-Rizzoli, P., Koh, T.Y., Song, G., 2014b. The relative importance of the wind-driven and tidal circulations in Malacca Strait. Cont. Shelf Res. 88, 92–102. http://dx.doi.org/10.1016/j.csr.2014.07.012.

DHI, 2007. Detailed studies on Tuas view extension and Pulau Tekong land reclamation, Malaysia and Singapore, DHI report eed-52745-DHI/15-10-2007.

Dietrich, J.C., Trahan, C.J., Howardb, M.T., Flemingc, J.G., Weaver, R.J., Tanakae, S., Yuf, L., Luettich, R.A., Dawsona, C.N., Westerinke, J.J., Wells, G., Luf, A., Vega, K., Kubachg, A., Dresback, K.M., Kolar, R.L., Kaiser, C., Twilley, R.R., 2012. Surface trajectories of oil transport along the Northern Coastal line of the Gulf of Mexico. Cont. Shelf Res. 41, 17–47. http://dx.doi.org/10.1016/j.csr.2012.03.015.

Egbert, G.D., Erofeeva, S.Y., 2002. Efficient inverse modeling of barotropic ocean tides. J. Atmos. Ocean. Technol. 19, 183204. http://dx.doi.org/10.1175/1520-0426(2002)019<0183:EIMOBO>2.0.CO;2.

Garcia-Martinez, R., Flores-Tovar, H., 2000. Computer modeling of oil spill trajectories with a high accuracy method. Spill Sci. Technol. Bull. 5, 323–330. http://dx.doi.org/10.1016/S1353-2561(99)00077-8.

Gianotti, R.L., 2013. Convective Cloud and Rainfall Processes Over the Maritime Continent: Simulation and Analysis of the Diurnal Cycle (Ph.D. Thesis). Massachusetts Institute of Technology.

Gianotti, R.L., Eltahir, E.A.B., 2014a. Regional climate modeling over the Maritime Continent. Part I: new parameterization for convective cloud fraction. J. Clim. 27, 1488–1503.

Gianotti, R.L., Eltahir, E.A.B., 2014b. Regional climate modeling over the Maritime Continent. Part II: new parameterization for autoconversion of convective rainfall. J. Clim. 27, 1504–1523.

Giese, B.S., Ray, S., 2011. El Niño variability in simple ocean data assimilation (SODA), 1871–2008. J. Geophys. Res. 116, C02024. http://dx.doi.org/10.1029/2010JC006695.

Gilbert, C.S., Gentleman, W.C., Johnson, C.L., DiBacco, C., Pringle, J.M., Chen, C., 2010. Modelling dispersal of sea scallop (Placopecten magellanicus) larvae on Georges Bank: the influence of depth-distribution, planktonic duration and spawning seasonality. Progress. Oceanogr. 87, 37–48. http://dx.doi.org/10.1016/j.pocean.2010.09.021.

Giorgi, F., Mearns, L.O., 1999. Introduction to special section: regional climate modeling revisited. J. Geophys. Res. 104, 6335–6352. http://dx.doi.org/10.1029/98JD02072.

Gordon, A.L., 2005. Oceanography of the Indonesian seas and their throughflow. Oceanography 18 (4), 14–27.

Gordon, A.L., Huber, B.A., Metzger, E.J., Susanto, R.D., Hurlburt, H.E., Adi, T.R., 2012. South China sea throughflow impact on the Indonesian throughflow. Geophys. Res. Lett. 39, L11602.

Hasan, G.M.J., van Maren, D.S., Cheong, H.F., 2012. Improving hydrodynamic modeling of an estuary in a mixed tidal regime by grid refining and aligning. Ocean Dyn.. http://dx.doi.org/10.1007/s10236-011-0506-4.

Hasan, G.M.J., van Maren, D.S., Ooi, S.K., 2016. Hydrodynamic modeling of Singapore's coastal waters: nesting and model accuracy. Ocean Model. 97, 141–151. http://dx.doi.org/10.1016/j.ocemod.2015.09.002.

Im, E., Marcella, M., Eltahir, E.A.B., 2014. Impact of potential large-scale irrigation on the West African monsoon and its dependence on location of irrigated area. J. Clim. 27, 994–1099.

Kajikawa, Y., Wang, B., 2012. Interdecadal change of the South China Sea summer monsoon onset. J. Clim. 25, 3207–3218. http://dx.doi.org/10.1175/JCLI-D-11-00207.1.

Kurniawan, A., Tay, S.H.X., Ooi, S.K., Babovic, V., Gerritsen, H., 2015. Analyzing the physics of non-tidal barotropic sea level anomaly events using multi-scale numerical modelling in Singapore regional waters. J. Hydro-Environ. Res. 9, 404–419. http://dx.doi.org/10.1016/j.jher.2014.10.0005.

Marcella, M., Eltahir, E.A.B., 2014c. Introducing an irrigation scheme to a regional climate model: a case study over West Africa. J. Clim. 27, 5708–5723.

Masumoto, Y., Sasaki, H., Kagimoto, T., Komori, N., Ishida, A., Sasai, Y., Miyama, T., Motoi, T., Mitsudera, H., Takahashi, K., Sakuma, H., Yamagata, T., 2004. A fifty-year eddy-resolving simulation of the world ocean-preliminary outcomes of OFES (OGCM for the earth simulator). J. Earth Simula. 1, 35–56.

National Center for Atmospheric Research Staff, 2016. (Eds). Last modified 13 Oct. "The Climate Data Guide: SODA: Simple Ocean Data Assimilation." Retrieved from ⟨https://climatedataguide.ucar.edu/climate-data/soda-simple-ocean-data-assimilation⟩.

Oliveira, L.A., Costa, V.A.F., Baliga, B.R., 2002. A Lagrangian–Eulerian model of particle dispersion in a turbulent plane mixing layer. Int. J. Numer. Methods Fluid, 40. http://dx.doi.org/10.1002/fld.366.

Pal, J.S., Giorgi, F., Bi, X., Elguindi, N., Solmon, F., Rauscher, S.A., Gao, X., Francisco, R., Zakey, A., Winter, J., Ashfaq, M., Syed, F.S., Sloan, L.C., Bell, J.L., Diffenbaugh,

N.S., Karmacharya, J.H., Konaré, A., Martinez, D., da Rocha, R.P., Steiner, A.L., 2007. Regional climate modeling for the developing world: The ICTP RegCM3 and RegCNET. Bull. Am. Meteorol. Soc. 88, 1395–1409. http://dx.doi.org/10.1175/BAMS-88-9-1395.

Pawlowicz, R., Beardsley, B., Lentz, S., 2002. Classical tidal harmonic analysis including error estimates in MATLAB using T_TIDE. Comput. Geosci. 28, 929–937.

Postma, H., Rommets, J.W., 1970. Primary production in the Wadden Sea. Neth. J. Sea Res. 4 (4), 470–493. http://dx.doi.org/10.1016/0077-7579(70)90009-8.

PUB (Singapore's National Water Agency), 2016. About Deep Tunnel Sewerage System, Accessed on March 20, 2016, url: ⟨https://www.pub.gov.sg/dtss⟩.

Qiu, Z., Doglioli, A.M., He, Y., Carlotti, F., 2011. Lagrangian model of zooplankton dispersion: numerical schemes comparisons and parameter sensitivity test. Chin. J. Oceanol. Limnol. 29, 438–445. http://dx.doi.org/10.1007/s00343-011-0015-9.

Russell, F.S., 1927. The vertical distribution of plankton in the sea. Biol. Rev. Camb. Philos. Soc. 2 (3), 213–262.

Sasaki, H., Nonaka, M., Masumoto, Y., Sasai, Y., Uehara, H., Sakuma, H., 2008. An eddy-resolving hindcast simulation of the quasiglobal ocean from 1950 to 2003 on the Earth Simulator. (chapter 10)In: Hamilton, K., Ohfuchi, W. (Eds.), High Resolution Numerical Modelling of the Atmosphere and Ocean. Springer, New York, 157–185.

Sien, C.L., Khan, H., Ming, C.L., 1988. The Coastal Environmental Profile of Singapore. Technical Publications Series 3, Asen, Jakarta/us Coastal Resources Management Project 88. Silver Spring, MD.

Singapore Statutes Online (SSO), 2008. Prevention of Pollution of the Sea Act (CHAPTER 243).

Sun, Y., Chen, C., Beardsley, R.C., Xu, Q., Qi, J., Lin, H., 2013. Impact of current-wave interaction on storm surge simulation: a case study for Hurricane Bob. J. Geophys. Res. 118, 2685–2701. http://dx.doi.org/10.1002/jgrc.20207.

Sun, Y., Chen, C., Beardsley, R.C., Ullman, D., Butman, B., Lin, H., 2016. Surface circulations in block Island sound and adjacent coastal and shelf regions: a FVCOM-CODAR comparison. Progress. Oceanogr. 143, 26–45. http://dx.doi.org/10.1016/j.pocean.2016.02.005.

Tay, S.H.X., Kurniawan, A., Ooi, S.K., Babovic, V., 2016. Sea level anomalies in straits of Malacca and Singapore. Appl. Ocean Res. 58, 104–117. http://dx.doi.org/10.1016/j.apor.2016.04.003.

The Maritime and Port Authority of Singapore (MPA), 2017. Port Statistics, Accessed on June 7, 2017, url: ⟨http://www.mpa.gov.sg/web/portal/home/port-of-singapore/port-statistics⟩.

Tian, R., Chen, C., Stokesbury, K.D.E., Rothschild, B.J., Xu, Q., Hu, S., Cowles, G., Harris, B.P., Marino II, M.C., 2009. Sensitivity analysis of sea scallop larvae trajectories to hydrodynamic model configuration on Georges Bank and adjacent coastal regions. Fish. Oceanogr. 18 (3), 173–184. http://dx.doi.org/10.1111/j.1365-2419.2009.00506.x.

Tremblay, M., Loder, J., Werner, F., Naimie, C., Page, F., Sinclair, M., 1994. Drift of sea scallop larvae Placopecten magellanicus on Geroges Bank: a model study of roles of mean advection, larval behavior and larval origin. Deep Sea Res. 41, 7–49. http://dx.doi.org/10.1016/0967-0645(94)90061-2.

Twigt, D.J., 2007. Seasonal, climatological boundary forcing for the Singapore regional model, Delft Hydraulics (Deltares) Research Report X0349, 21.

Valcke, S., 2013. The OASIS3 coupler: a European climate modelling community software. Geosci. Model Dev. 6, 373–388. http://dx.doi.org/10.5194/gmd-6-373-2013.

van Maren, D.S., Gerritsen, H., 2012. Residual flow and tidal asymmetry in the Singapore Strait, with implications for resuspension and residual transport of sediment. J. Geophys. Res.: Oceans 117, 2156–2202. http://dx.doi.org/10.1029/2011JC007615.

Watanabe, T., Yamazaki, K., 2014. Decadal-scale variation of south asian summer monsoon onset and its relationship with the pacific decadal oscillation. J. Clim., (doi:/10.1175/JCLI-D-13-00541.1).

Wei, J., Malanotte-Rizzoli, P., Eltahir, E.A.B., Xue, P., Zhang, D., 2013. Coupling of a regional atmospheric model (RegCM3) and a regional oceanic model (FVCOM) over the maritime continent. Clim. Dyn.. http://dx.doi.org/10.1007/s00382-013-1986-3.

Winter, J.M., Pal, J.S., Eltahir, E.A.B., 2009. Coupling of integrated biosphere simulator to regional climate model version 3. J. Clim. 22, 2743–2756.

Xu, M., Chua, V.P., 2016. A numerical study on flow and pollutant transport in Singapore coastal waters. Mar. Pollut. Bull.. http://dx.doi.org/10.1016/j.marpolbul.2016.07.014.

Xue, P., Eltahir, E.A.B., Malanotte-Rizzoli, P., Wei, J., 2014. Local feedback mechanisms of the shallow water region around the maritime continent. J. Geophys. Res.. http://dx.doi.org/10.1002/2013JC009700.